Model-Predictive Cascade Mitigation in Electric Power Systems With Storage and Renewables, Part I: Theory and Implementation

Mads Almassalkhi, *Student Member, IEEE*   Ian Hiskens, *Fellow, IEEE*

Abstract—A novel model predictive control (MPC) scheme is developed for mitigating the effects of severe line-overload disturbances in electrical power systems. A piece-wise linear convex approximation of line losses is employed to model the effect of transmission line power flow on conductor temperatures. Control is achieved through a receding-horizon model predictive control (MPC) strategy which alleviates line temperature overloads and thereby prevents the propagation of outages. The MPC strategy adjusts line flows by rescheduling generation, energy storage and controllable load, while taking into account ramp-rate limits and network limitations. In [1], the MPC strategy is illustrated through simulation of the IEEE RTS-96 network, augmented to incorporate energy storage and renewable generation.

Index Terms—Cascade mitigation, convex relaxation, energy storage, modeling, model predictive control, optimization, thermal overloads.

I. INTRODUCTION

THE National Academy of Engineering named the electric power grid the greatest engineering achievement of the 20th century [2]. However, recent large-scale power grid failures suggest the electric grid is becoming increasingly congested, and as a consequence, is being operated closer and closer to its limits [3].

Currently, abnormal conditions are handled either through protection operation or operator intervention, depending on the severity of the abnormality. In the latter case, where conditions do not immediately threaten the integrity of plant or loads, operators institute corrective procedures that may include altering generation schedules, adjusting transformer tap positions, and switching capacitors/reactors. For more extreme abnormalities, the protection associated with vulnerable components will operate to ensure they do not suffer damage. This myopic response may, however, weaken the network, exacerbating the conditions experienced by other components. They may subsequently trip, initiating an uncontrolled cascade of outages. This pattern was exhibited during the blackout of the U.S. and Canada in August 2003 [4].

As the amount, type and distribution of controllable resources increases, operators will find it ever more challenging to determine an appropriate response to unanticipated events. At a minimum, operators will require new tools to guide their decision-making. Given the increased complexity of response actions, a closed-loop feedback process will become indispensable. Furthermore, since power systems are suffused with constraints and limits on states and inputs, model predictive control (MPC) schemes can be particularly useful within the

context of contingency management. For a general overview of MPC, see [5], [6], [7].

The first application of MPC to emergency control of power systems was [8], where voltage stability was achieved through optimal coordination of load shedding, capacitor switching, and tap-changer operation. A tree-based search method was employed to obtain optimal control actions from discrete switching events. To circumvent tree-based search methods, [9], [10] employed trajectory sensitivities to develop MPC strategies. However, those methods focused on voltage stability and did not take into account energy storage nor thermal overloads of transmission lines. Distributed forms of MPC have also been proposed, with mitigation of line-outage cascades considered in [11].

The authors in [12], [13] proposed a framework for electrothermal coordination in power systems, and developed temperature-based predictive algorithms that are amenable to energy markets and applicable within existing system controls. Other recent literature, cf. [14], [15], focused on model-predictive control of electrical energy systems to alleviate line overloads within a standard DC power flow framework. Specifically, the authors in [15] extended the ideas of [14] to include a linearized current-based thermodynamical model of conductors and an auto-regressive model of the weather conditions (i.e. wind speed and ambient temperature) near transmission lines. This allowed [15] to set a hard upper limit on conductor temperature to ensure control objectives, and allowed MPC to operate the system closer to actual physical limits than if using standard (worst-case weather-based) thermal ratings. Furthermore, [15] illustrated that temperature-based control can outperform current control within a predictive framework.

The control scheme developed in this paper is motivated by the bilevel control structure that was introduced in [16] for large-scale energy-hub systems. The first level operated on an hour-by-hour timescale with a 24-hour prediction horizon and was in charge of economic dispatch. The second level responded to contingencies and was implemented as a simple deterministic shrinking (fixed-point) horizon model predictive cascade mitigation scheme, which shed minimal load in the process of halting the cascade. The effectiveness of the cascade mitigation process in maximizing economic and secure operation was due to proper management of available energy storage and renewable energy sources. The impact of different energy storage scenarios on cascade mitigation was investigated in [17], where it was concluded that the MPC scheme alone provided considerable protection against cascade failures and that appropriate storage schemes further improved performance. However, the use of shrinking horizon MPC in [16] required that the system recover from the initial outage by the fixed terminal time, potentially leaving
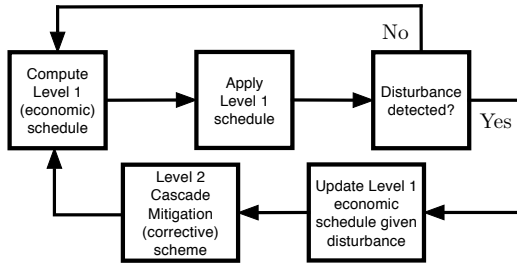
Fig. 1. Overview of proposed control scheme showing Level 1 (economical) and Level 2 (corrective) interaction.

insufficient time to respond to late disturbances. Therefore, to improve robustness, this paper extends [16] by implementing a receding-horizon MPC scheme (henceforth referred to simply as MPC).

The main contribution of this paper is the formulation of a linear MPC scheme for bulk power systems, which balances economic and security objectives, thereby driving the system to a secure and economical operating region. In addition, the paper develops a piece-wise linear convex relaxation for branch losses that significantly reduces the computational complexity of the optimization problem underpinning MPC. The resulting MPC scheme exploits the thermal inertia inherent in transmission line conductors to allow time for controllable resources, including generation and energy storage, to reschedule, thereby alleviating line overloads and mitigating cascading failures. The proposed approach represents a departure from current practice because it envisions a corrective control strategy that shifts the operating paradigm of power systems from "generation follows load" to "energy positioning".

This paper (Part I) motivates and develops the MPC framework, while the benefits of the proposed approach are illustrated in Part II [1], where the IEEE RTS-96 system forms the basis for a contingency management case-study. The remainder of this paper is organized as follows. Section II establishes the proposed two-level control framework, and discusses the roles of Levels 1 and 2, and their interactions. The Level 2 (MPC) controller model, including a convex relaxation of line losses, is developed in Section III. Section IV summarizes the paper and suggests future research directions.

II. System Operation and Control

Economic dispatch computes an economically optimal trajectory, for a given load forecast. However, if a significant disturbance takes place, it may be necessary to operate suboptimally for some time to prevent overloads and minimize the risk of subsequent line outages. This motivates the need for a contingency (safety) controller, which responds quickly to a disturbance, and subsequently drives the system back to a secure and economical state. From that state, economic dispatch can be re-initiated and normal (economic) operation can resume. This suggests a bilevel hierarchical control strategy for electric power systems. Fig. 1 provides an overview of the proposed bilevel hierarchical operation of the system. A discussion of each level follows.

A. Level 1: Optimal energy schedule

Level 1 uses forecasts of load demand and renewable resources to compute an optimal 24-hour ahead schedule for energy storage, conventional generation, flexible loads, and available renewable energy. This scheduling process is similar to standard economic dispatch [18], though the dynamics (and hence temporal coupling) introduced by energy storage state-of-charge and generator ramp-rate limits must be taken into account. This implies optimization over a horizon rather than a single time-step.

The Level 1 model enforces line flow (thermal) limits to ensure that, under accurate model and forecast scenarios, no lines are overloaded (i.e. the system is secure). Line losses are modeled with a standard piece-wise linear (PWL) DC approximation as presented in [19]. The dispatch schedule is computed as a multi-period quadratic programming (QP) problem whose objective is to minimize energy (fuel) costs of conventional generators:

$$\text{Cost}\big(f_{Gn}[k]\big) = a_n\big(f_{Gn}[k]\big)^2 + b_n f_{Gn}[k] \qquad (1)$$

where a_n [\$/h-pu^2] and b_n [\$/h-pu] are constant parameters for generator n, and f_{Gn} [pu] is its output power.

The Level 1 schedule establishes a reference signal over a multi-hour horizon, consisting of the economically optimal system set-points x^{sp}, and the operator control actions u^{sp} required to achieve those optimal set-points. The schedule is submitted to the operator and recomputed every hour. For details on the Level 1 formulation, see [16], [20].

Remark II.1. Level 1 may take advantage of existing energy management system (EMS) tools to assess voltage conditions and identify corrective behavior [21], [22]. Required actions can be encapsulated in the set-points submitted to Level 2. Then, Level 2 can focus on resolving short-term line overloads while driving the system to a long-term voltage secure and economically optimal state.

Online monitoring of voltage conditions may necessitate reconfiguring network limits and modifying set-points for Level 2. This could be achieved by considering real-time measurements from phasor measurement units, see for example [23]. Such schemes are beyond the scope of this paper, though are identified as future work in Section IV.

B. Level 2: Corrective control

This lower level controller operates in the background to track the reference trajectories computed by Level 1 (i.e. the economic set-point values). Since the Level 2 time-step T_s (≈ 1 minute) is much shorter than that of the Level 1 reference signals (≈ 1 hour), linear interpolation is employed between state reference values, while a zero-order-hold is used for control reference values[1].

---

[1]Assume the Level 1 time-step is KT_s, and consider two adjacent Level 1 state reference values $\hat{x}_i^{\text{sp}}$ and $\hat{x}_{i+1}^{\text{sp}}$. Then the value of the Level 2 state reference at time kT_s, between $\hat{x}_i^{\text{sp}}$ and $\hat{x}_{i+1}^{\text{sp}}$, is $x_k^{\text{sp}} = \frac{k}{K}(\hat{x}_{i+1}^{\text{sp}} - \hat{x}_i^{\text{sp}}) + \hat{x}_i^{\text{sp}}$, $k = 0, ..., K$. If the corresponding Level 1 control reference values are $\hat{u}_i^{\text{sp}}$ and $\hat{u}_{i+1}^{\text{sp}}$, then the Level 2 control references take the values $u_k^{\text{sp}} = \hat{u}_i^{\text{sp}}$, $k = 0, ..., K-1$ and $u_K^{\text{sp}} = \hat{u}_{i+1}^{\text{sp}}$.

The corrective controller employs a linear model of the actual system. If a disturbance takes place (e.g. line outage), Level 2 uses MPC to compute corrective control actions that steer the system towards a safe and economically optimal state as provided by the Level 1 post-disturbance reference.

Level 2 relies on a discrete-time model of the system. Discrete dynamics are obtained by forward Euler discretization with sample time T_s. Controls are step-wise, with step-width T_s, such that $u(t) := u[k]$ for $t \in [kT_s, (k+1)T_s)$. For each time k, the dynamic states x_k^{meas} are measured and represent the initial state of the system. The MPC scheme can be summarized as follows:

1) At time k, with initial states x_k^{meas} and updated Level 1 reference signals x_k^{sp} and u_k^{sp}, solve an open-loop optimal control problem over the interval $[k, k+M]$ taking into account current and future constraints. This yields a sequence of optimal open-loop control actions $\{u[0|k], u[1|k], \ldots, u[M-1|k]\}$, where the notation $[l|k]$ implies prediction time l relative to the actual time k.
2) Apply the first instance of the control sequence: $u[k] := u[0|k]$.
3) Measure the actual system state x_{k+1}^{meas} at time $k+1$.
4) Set $k = k+1$ and repeat step 1).

Level 2 considers ramp-rate limits on conventional generators, dynamics and power ratings of grid storage devices, and incorporates the thermal response of overloaded lines. Note that in Level 2, lines are no longer necessarily subject to a hard flow-limit constraint. Rather, the controller seeks to drive line temperatures below their respective limits. The Level 2 open-loop MPC optimization is formulated as a quadratic programming problem (QP) over the finite prediction horizon M:

$$\min_{u[l|k]} \left|\left| x[M|k] - x_{k+M}^{\text{sp}} \right|\right|_{S_M} + \sum_{l=0}^{M-1} L\left(x[l|k], u[l|k]\right) \quad (2a)$$

$$\text{s.t.} \quad x[l+1|k] = Ax[l|k] + Bu[l|k] + Fz[l|k] \quad (2b)$$

$$0 = \hat{A}x[l|k] + \hat{B}u[l|k] + \hat{F}z[l|k] \quad (2c)$$

$$Cx[l|k] + Du[l|k] + Gz[l|k] \le d \quad (2d)$$

$$x[l|k] \in \mathcal{X}, \ u[l|k] \in \mathcal{U}, z[l|k] \in \mathcal{Z} \quad (2e)$$

$$x[M|k] \in \mathcal{T}_x \quad (2f)$$

$$x[0|k] = x_k^{\text{meas}} \quad (2g)$$

where $x[l|k]$, $u[l|k]$, and $z[l|k]$ represent the dynamic state, control input, and algebraic state variables, respectively, at predicted time $0 \le l < M$, given initial measured state x_k^{meas} at time k. The appropriately-sized matrices A, B, F and $\hat{A}, \hat{B}, \hat{F}, C, D, G$ describe dynamic and algebraic constraints, respectively. The objective function in (2a) is defined by:

$$L(x[l|k], u[l|k]) = ||x[l|k] - x_{k+l}^{\text{sp}}||_Q + ||u[l|k] - u_{k+l}^{\text{sp}}||_R \quad (3)$$

where x_{k+l}^{sp} and u_{k+l}^{sp} refer to the Level 1 trajectory interpolated at time $k+l$, the norms are defined by $||y||_B \equiv y^\top B y$, and weighting matrices $S_M \succeq 0$ and $Q \succeq 0$ are non-negative definite while $R \succ 0$ is positive definite. Expressions (2b) and (2c) describe the differential-algebraic (DAE) dynamics. Expressions (2d), (2e), and (2f) define static inequality constraints, bounds on states and inputs, and a terminal state

constraint set, respectively. Equation (2g) establishes the initial state for MPC. The details of the Level 2 MPC system model are developed and discussed in Section III.

III. CONTROLLER MODEL

An electric power system network can be described in a graph-theoretic sense as consisting of a set of nodes and edges, (i.e. edge $e_l = (i, j) \in \mathcal{E}$ for nodes $i, j \in \mathcal{N}$). The physics that explicitly relate the nodes and the edges of the network must be considered. Physical power flows in an electric network are generally modeled with the nonlinear, non-convex AC power flow [18]. In order to circumvent issues associated with non-convexity, the Level 2 MPC controller utilizes a simplified but sufficient linear (i.e. "DC") power flow model.

In subsequent model developments, the index $l \in \mathcal{M} := \{0, \ldots, M-1\}$ denotes discrete time-steps, and the MPC scheme is employed with prediction and control horizon M. For notational convenience, the time index l is excluded for constraints that are point-wise in time.

A. Unified DC power flow

A large power system may consist of multiple interconnections between differing voltage levels. In order to include the effects of in-phase (IPT) and phase-shifting (PST) transformers on branch flows, a "Unified Branch Model", developed in [24] and illustrated in Fig. 2, is employed. In the standard way, line impedance Z_{ij} and admittance Y_{ij} are related through:

$$Z_{ij} = r_{ij} + \imath x_{ij} \implies Y_{ij} = \frac{1}{Z_{ij}} = g_{ij} + \imath b_{ij} \quad (4)$$

where $r_{ij}, x_{ij}, g_{ij}, b_{ij}$ are line resistance, reactance, conductance and susceptance, respectively. Define the complex voltage at node i as $V_i = U_i \underline{/\theta_i}$ and complex transformer tap-ratio as $t_{ij} = a_{ij} \underline{/\psi_{ij}}$. This allows a unified representation for transmission lines ($a_{ij} = 1$, $\psi_{ij} = 0$), IPTs ($y_{ij}^{\text{sh}} = y_{ji}^{\text{sh}} = 0$, $\psi_{ij} = 0$), and PSTs ($y_{ij}^{\text{sh}} = y_{ji}^{\text{sh}} = 0$, $a_{ij} = 1$). Using standard DC assumptions:

- $|V_i| = U_i \approx 1$ pu,
- $|\theta_{ij} - \psi_{ij}| \ll \pi/2$,
- losses are negligible (i.e. $g_{ij} \approx 0$), and
- reactance is much greater than resistance ($x_{ij} \ge 4r_{ij}$),

the AC (nonlinear) expression for active power flow can be simplified to give a "unified DC model":

$$f_{ij} \approx \frac{\theta_{ij} - \psi_{ij}}{a_{ij}x_{ij}} = \frac{\hat{\theta}_{ij}}{\hat{x}_{ij}} \quad (5)$$

where $\hat{\theta}_{ij} = \theta_{ij} - \psi_{ij}$, $\hat{x}_{ij} = a_{ij}x_{ij}$, and f_{ij} is the active power flowing from node i to node j. Note that the expression (5) is similar to a standard DC transmission line branch model, except that the phase-shift and tap turns-ratio modify the standard phase-angle difference and reactance terms, respectively. To maintain linearity in the model, assume a_{ij} is a constant parameter over the prediction horizon.

Remark III.1. The unified DC model retains the ability of PSTs to direct line flow via ψ_{ij}. This affords the proposed MPC scheme additional control of networks with PSTs.
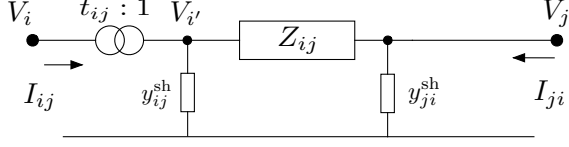
Fig. 2. The unified branch model (π-model) with complex voltages, currents, taps, admittance, and shunts.

B. Line losses

1) Derivation of line losses for the DC power flow: The unified DC power flow model presented above ignores active line losses. However, to alleviate temperature overloads caused by ohmic heating in transmission lines, it is necessary for the MPC controller to model I^2R line losses. To establish a relationship for losses on branch (i, j), the AC expression for active power flow can be manipulated to give:

$$f_{ij}^{\text{loss}} = f_{ij} + f_{ji} = g_{ij}\left(\frac{U_i^2}{a_{ij}^2} + U_j^2 - 2\frac{U_i}{a_{ij}}U_j\cos\hat{\theta}_{ij}\right). \quad (6)$$

Assuming voltage magnitudes are close to 1 pu and approximating $\cos\hat{\theta}_{ij}$ by a second-order Taylor series expansion gives,

$$f_{ij}^{\text{loss}} \approx g_{ij}\left(\frac{1}{a_{ij}^2} + 1 - \frac{2}{a_{ij}}\cos\hat{\theta}_{ij}\right) \quad (7)$$

$$\approx g_{ij}\left(\left(\frac{1}{a_{ij}} - 1\right)^2 + \frac{\hat{\theta}_{ij}^2}{a_{ij}}\right). \quad (8)$$

Furthermore, assuming the nominal tap ratio $a_{ij} \approx 1$ gives,

$$f_{ij}^{\text{loss}} \approx g_{ij}\frac{\hat{\theta}_{ij}^2}{a_{ij}} = \frac{r_{ij}}{r_{ij}^2 + x_{ij}^2}\frac{\hat{\theta}_{ij}^2}{a_{ij}} \approx \frac{r_{ij}}{x_{ij}^2}\frac{\hat{\theta}_{ij}^2}{a_{ij}}, \quad (9)$$

where the final step follows because $x_{ij} \geq 4r_{ij}$ for most transmission lines. Thus, the unified "DC" line losses can be written:

$$f_{ij}^{\text{loss}} \approx \frac{r_{ij}\hat{\theta}_{ij}^2}{a_{ij}x_{ij}^2} = a_{ij}\,r_{ij}\,f_{ij}^2, \quad (10)$$

with the unified DC flow f_{ij} defined in (5). Note that the loss term f_{ij}^{loss} is quadratic in $\hat{\theta}_{ij}$ and is therefore not suitable for the strictly linear constraint formulation. A meaningful model of losses can be incorporated into this formulation by applying a (piece-wise) linear approximation of losses that circumvents the need for integer optimization, see [19], [25].

Remark III.2. For lines with $a_{ij} \equiv 1$ (e.g. without transformers), the PWL approximation can be applied directly to the term $\cos\hat{\theta}_{ij}$, rather than its Taylor series expansion. In cases where $a_{ij} \neq 1$, though, a PWL approximation of the term $\cos\hat{\theta}_{ij}$ gives $\hat{\theta}_{ij} = 0 \Rightarrow f_{ij}^{\text{loss}} = (1 - 1/a_{ij})^2 > 0$, which does not represent a standard DC relationship between phase-angle difference and flow. In contrast, (10) satisfies the standard DC relationship $\hat{\theta}_{ij} = 0 \Rightarrow f_{ij} + f_{ij}^{\text{loss}} = 0$. Thus, to simplify notation and maintain a unified line-loss model, (10) is employed throughout the paper.
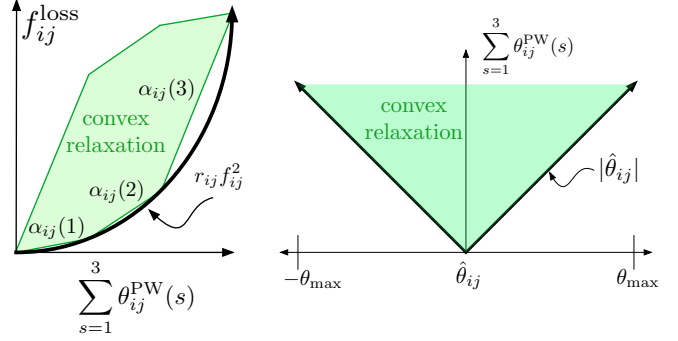
(a) PWL adjacency relaxation.

(b) Absolute value relaxation.

Fig. 3. Relaxing adjacency conditions and absolute value complementarity condition (i.e. $\theta_{ij}^{+}\theta_{ij}^{-} = 0$) for PWL approximation with $S = 3$.

2) PWL approximation of line losses: The approximate losses in (10) can be replaced by a piece-wise linear (PWL) formulation consisting of S linear segments of width $\Delta\theta$, as indicated in Fig. 3a. To represent (10), the slope of each segment is given by:

$$\alpha_{ij}(s) = (2s - 1)\frac{r_{ij}}{a_{ij}x_{ij}^2}\Delta\theta, \quad \forall s \in \{1, \ldots, S\}. \quad (11)$$

Define the variables $\theta_{ij}^{\text{PW}}(s) \in [0, \Delta\theta]$, $\forall s \in \{1, \ldots, S\}$, such that:

$$|\hat{\theta}_{ij}| = \sum_{s=1}^{S}\theta_{ij}^{\text{PW}}(s). \quad (12)$$

Then the loss formulation (10) can be approximated by:

$$f_{ij}^{\text{loss}} \approx \text{PWL}\left[\frac{r_{ij}}{a_{ij}x_{ij}^2}|\hat{\theta}_{ij}|^2\right] = \sum_{s=1}^{S}\alpha_{ij}(s)\theta_{ij}^{\text{PW}}(s), \quad (13)$$

where PWL$[\cdot]$ denotes the piece-wise linear approximation. Implementation of PWL$[\cdot]$ within an optimization framework generally requires binary integers to enforce adjacency conditions for the PWL segments [26]. Adjacency conditions ensure that if $\theta_{ij}^{\text{PW}}(s) > 0$ then $\theta_{ij}^{\text{PW}}(p) = \Delta\theta$, $\forall p < s$. However omitting integers and relaxing the adjacency conditions gives a strictly continuous linear approximation of line losses that is equivalent to a bounded convex relaxation of PWL$[\cdot]$:

$$\text{PWL}\left[\frac{r_{ij}}{a_{ij}x_{ij}^2}|\hat{\theta}_{ij}|^2\right] \leq \sum_{s=1}^{S}\alpha_{ij}(s)\theta_{ij}^{\text{PW}}(s) \equiv f_{ij}^{\text{loss}}, \quad (14)$$

where f_{ij}^{loss} now gives the relaxed value of the computed losses. This linear relaxation is convex. Because (7) is strictly locally convex for $\theta_{ij} \in (-\pi/2, \pi/2)$ and $r_{ij}, x_{ij}, a_{ij} > 0$, the segment slopes satisfy $\alpha_{ij}(s) < \alpha_{ij}(s + 1)$ and are therefore monotonically increasing. This is illustrated in Fig. 3a for $S = 3$. Note that with the adjacency condition relaxed, f_{ij}^{loss} can take any value in the convex space labeled "convex relaxation" in Fig. 3a.

The (non-convex) absolute value constraint in (12) can be incorporated into the linear formulation using the standard

relaxation:

$$\hat{\theta}_{ij} = \theta_{ij}^+ - \theta_{ij}^- \qquad (15)$$

$$\sum_{s=1}^{S} \theta_{ij}^{\text{PW}}(s) := \theta_{ij}^+ + \theta_{ij}^- \qquad (16)$$

where $\theta_{ij}^+, \theta_{ij}^- \geq 0$. This is equivalent to a bounded convex relaxation, since $|\hat{\theta}_{ij}| = |\theta_{ij}^+ - \theta_{ij}^-| \leq |\theta_{ij}^+| + |\theta_{ij}^-| = \theta_{ij}^+ + \theta_{ij}^-$, which is demonstrated in Fig. 3b.

Remark III.3. To ensure $|\hat{\theta}_{ij}| = \theta_{ij}^+ + \theta_{ij}^-$, the complementarity condition $0 \leq \theta_{ij}^- \perp \theta_{ij}^+ \geq 0$ must be enforced. Otherwise, the absolute-value relaxation (15)-(16) may overestimate absolute phase-angle values. Complementarity can be achieved using a mixed-integer formulation:

$$0 \leq \theta_{ij}^+ \leq z_{ij}\theta_{\max}, \quad 0 \leq \theta_{ij}^- \leq (1-z_{ij})\theta_{\max}, \quad z_{ij} \in \{0,1\}.$$

However, integer implementation prevents a strictly QP formulation of line losses, and is not pursued. Rather, it is proven in Theorem III.8 that explicit enforcement of complementarity is unnecessary.

To summarize, the convex relaxation of active line losses is described by the following relations:

$$f_{ij}^{\text{loss}} := \frac{r_{ij}}{a_{ij}x_{ij}^2}\Delta\theta \sum_{s=1}^{S}(2s-1)\theta_{ij}^{\text{PW}}(s) \qquad (17a)$$

$$\sum_{s=1}^{S} \theta_{ij}^{\text{PW}}(s) = \theta_{ij}^+ + \theta_{ij}^- \qquad (17b)$$

$$\hat{\theta}_{ij} \equiv \theta_{ij} - \psi_{ij} = \theta_{ij}^+ - \theta_{ij}^- \qquad (17c)$$

$$\hat{\theta}_{ij} \in (-\theta_{\max}, \theta_{\max}) \qquad (17d)$$

$$0 \leq \theta_{ij}^+, \theta_{ij}^- \qquad (17e)$$

$$\theta_{ij}^{\text{PW}}(s) \in [0, \Delta\theta]. \qquad (17f)$$

The linear constraint formulation presented in (17) is a convex relaxation of a lossy DC power flow, and gives a value for f_{ij}^{loss} that is greater than or equal to the piecewise linear approximation PWL[·] given by (13). Equality occurs only when both absolute value complementarity (i.e. $\theta_{ij}^+ \theta_{ij}^- = 0$) and PWL adjacency conditions are satisfied. Under such conditions, the relaxation is considered "tight" and the model is exact (i.e. equality is achieved in (14)). When the losses are relaxed (i.e. not tight), overestimated losses are denoted "fictitious losses", as they exist only as an artifact of the MPC controller model and not in the actual system.

Remark III.4. Theorem III.8 and Appendix B establish a sufficient condition that ensures a tight relaxation. Under tight conditions, the convex relaxation of line losses provides a more accurate method for estimating line losses than standard linearization.

C. Generation, load, storage, and power balance

For conventional (controllable) generator n, the injections are denoted f_{Gn}, with ramp-rate limits R_n^{up} and R_n^{down} [pu/s].

The following constraints are included in the controller model:

$$f_{Gn}[l+1] = f_{Gn}[l] + \Delta f_{Gn}[l] \qquad (18a)$$

$$f_{Gn} \in [\underline{f_{G_n}}, \overline{f_{Gn}}], \quad \Delta f_{Gn} \in [-T_s R_n^{\text{down}}, T_s R_n^{\text{up}}]. \qquad (18b)$$

The discrete-time equation (18a), with sampling time (i.e. time-step width) T_s, represents the dynamics of generator ramping.

Power injections from non-dispatchable wind-turbine generator n, $f_{G_W n}$, are not subject to ramp-rate conditions but may be curtailed (i.e. spilled) from their (forecast and actual) nominal output level:

$$f_{G_W n} = f_{G_W n}^{\text{nom}} - f_{G_W n}^{\text{spill}}, \qquad f_{G_W n}^{\text{spill}} \in [0, \alpha_n^{\text{spill}}] \qquad (19)$$

where $f_{G_W n}^{\text{spill}}$ represents the controlled reduction from the nominal available wind power.

It is assumed that load n is (partially) controllable through fast-acting demand response schemes. That is, for all loads n,

$$f_{Dn} = f_{Dn}^{\text{nom}} - f_{Dn}^{\text{red}}, \qquad f_{Dn}^{\text{red}} \in [0, \alpha_n^{\text{red}}], \qquad (20)$$

where f_{Dn}^{nom} is the nominal (forecast and actual) load and f_{Dn}^{red} represents the reduction in nominal load.

Energy storage is also available (e.g. grid-scale battery systems, pumped hydro, hydrogen fuel cells), with energy storage devices located at various nodes throughout the network. The state of charge (SOC) of the n-th energy storage device, $E_n[l] \in [0, \overline{E}_n]$, is defined by the discrete dynamics:

$$E_n[l+1] = E_n[l] + T_s\eta_{c,n}f_{Qc,n}[l] - \frac{T_s}{\eta_{d,n}}f_{Qd,n}[l], \qquad (21)$$

where $\eta_{c,n}$ ($\eta_{d,n}$) is the constant charging (discharging) efficiency of device n. Charging and discharging rates are limited according to $f_{Qc,n} \in [0, \overline{f_{Qc,n}}]$, $f_{Qd,n} \in [0, \overline{f_{Qd,n}}]$. The total power injected by storage device n is $f_{Qn} = f_{Qc,n} - f_{Qd,n}$, where $f_{Qn} > 0$ ($f_{Qn} < 0$) represent charging (discharging) behavior.

Remark III.5. This model permits simultaneous charging and discharging. While this is mathematically *feasible*, it is generally not physically *realizable* (i.e. some hydro-storage can simultaneously charge/discharge, but most electrical storage devices cannot). A more accurate energy storage model would employ the complementarity condition $f_{Qc,n}[l]f_{Qd,n}[l] = 0$, but that results in a difficult nonlinear model [27]. Instead of applying an integer-based approach to model the complementarity condition (see Remark III.3), the MPC model relaxes complementarity. This introduces modeling inaccuracy between plant and controller that is proportional to $1 - \eta_{c,n}\eta_{d,n}$. However, as discussed in Appendix A, a heuristic algorithm can be employed to reduce the occurrence and effects of simultaneous charge/discharge events. Any remaining modeling inaccuracy is rejected through the feedback process, as evidenced in [1].

Networks must satisfy Kirchhoff's laws, which implies that the net power flow into any node must equal the net flow out. Generators (loads) may inject (consume) power at a node. If energy storage devices are available at a node, then discharging

(charging) corresponds to additional injections (demands). The power balance equation at each node $i \in \mathcal{N}$ is formulated as:

$$\sum_{n \in \Omega_i^{\text{G}}} f_{Gn} - \sum_{j \in \Omega_i^{\text{N}}} f_{ij}^{\text{T}} - \sum_{n \in \Omega_i^{\text{E}}} f_{Qn} - \sum_{n \in \Omega_i^{\text{D}}} f_{Dn} = 0 \qquad (22)$$

where $f_{ij}^{\text{T}} = f_{ij} + \frac{1}{2} f_{ij}^{\text{loss}}$ is the total flow on line (i,j) and
- Ω_i^{G} – set of generators at node i (wind and conventional)
- Ω_i^{N} – set of nodes adjacent to node i
- Ω_i^{D} – set of demands at node i
- Ω_i^{E} – set of energy storage devices at node i.

As well as contributing to the power balance (22), line losses f_{ij}^{loss} also drive the temperature dynamics associated with line overloads. This dual role must be carefully considered to ensure a tight formulation of the PWL approximation.

Remark III.6. (Fixing losses over the prediction horizon.) Under the standard convex relaxation of a PWL approximation of line-losses [19], it is implicitly assumed, for tightness of the formulation, that nodal prices (i.e. LMPs) are non-negative. Negative nodal prices arise for nodes where increasing power consumption leads to decreased overall system costs. For example, if a line is congested or trips at time k and forces a generator at node i to decrease output (i.e. $f_{Gn}[k] - f_{Gn}[k-1] < 0$ for $n \in \Omega_i^{\text{G}}$), then it can be shown that the nodal price at that node at time k will become negative. This breaks the assumption of non-negative nodal prices and prevents a tight formulation of losses. Fictitious losses can then "consume" power via the power balance equation (for nodes with negative LMPs) and reduce the overall objective function value. Similar but more thorough conclusions have been reached by authors in [25], [28] in relation to convex relaxations in power systems.

To overcome the challenge of negative LMPs, losses are fixed in (22), with line flows given by:

$$f_{ij}^{\text{T}} = f_{ij} + \frac{1}{2} f_{ij,k}^{\text{loss,est}} \qquad (23)$$

where $f_{ij,k}^{\text{loss,est}}$ is obtained from the state estimate of the AC system at time k, (i.e. the initial point of the MPC horizon.) The proof of tightness of the convex relaxation, given in Appendix B does not, therefore, require consideration of nodal prices. Furthermore, by fixing losses in the power balance equation, the network structure does not affect the convex relaxation.

It should be emphasized that losses are not omitted from (22), but rather are held constant through (23). Therefore, only the variation in losses over the prediction horizon is neglected. As the system settles to its post-disturbance steady-state, this loss variation approaches zero and the approximation disappears.

D. Line overloads

Protection schemes, such as over-current relays, detect abnormal conditions and trip affected components (i.e. remove them from service.) These devices operate automatically on a sub-second timescale and are, therefore, not considered in this work. Rather, this paper considers a time-scale of minutes, which shifts the focus from fault conditions to thermal considerations of transmission line conductors and sagging.

Transmission lines have prescribed power flow limits to prevent dangerous sagging and permanent conductor damage. These limits are related to the thermal capacity of the conductors and their ability to dissipate heat arising from resistive losses. Generally, there is an inverse relationship between the current flow on a line and the time allowed before the line must be taken out of service. In most common overload scenarios, this time response is on the order of 10-20 minutes.

Let $f_{ij}^{\text{lim}} > 0$ be the (3-phase MVA) thermal limit on line (i,j). To ensure secure line flows, it is desirable for an operator to enforce:

$$|f_{ij}| + \frac{1}{2} f_{ij}^{\text{loss}} \leq f_{ij}^{\text{lim}} \qquad \forall (i,j). \qquad (24)$$

While it is feasible to take inequality (24) into consideration in determining an hourly energy dispatch schedule (i.e. Level 1), it is unrealistic to expect such a constraint to be enforced immediately following a significant disturbance (e.g. line outage). This is because power flows depend on the physics of the network and are uncontrollable in the short term. Consequently line flows may temporarily exceed their limits following contingencies. Therefore, in the Level 2 control strategy, line overloads are tracked via the conductor temperature, and the controller seeks to alleviate sustained temperature overloads.

To model conductor temperature, the IEEE Standard 738 [29] for calculating the current-temperature relations of bare overhead conductors was employed. Consider an overhead conductor as a per-unit length thermal mass with continuous-time temperature dynamics:

$$\dot{T}(t) = \frac{1}{mC_p} \Big(q_s(t) + f_{ij}^{\text{loss}}(t) - \eta_c \big(T(t) - T_{\text{amb}}(t) \big)$$
$$- \eta_r \big((T(t) + 273)^4 - (T_{\text{amb}}(t) + 273)^4 \big) \Big) \qquad (25)$$

where T and T_{amb} are the conductor and ambient temperatures [°C], respectively, and f_{ij}^{loss} is the active power loss per unit length [W/m] in conductor (i,j), calculated according to (17). Values $mC_p, q_s, \eta_c,$ and η_r represent per unit length conductor heat capacity [J/m-°C], solar heat gain rate [W/m], conductive heat loss rate coefficient [W/m-°C], and radiative heat loss rate coefficient [W/m-°C^4], respectively. Coefficients η_c, η_r depend on the conductor characteristics. Besides the variation in resistance with conductor temperature, nonlinearities arise from the radiative heat losses. However, for conductor temperatures below 100°C, it is approximately linear.

To allow for tractable implementation of the MPC scheme, (25) is discretized and linearized around the equilibrium point $T^* = T^{\text{lim}}$, where T^{lim} is computed from steady-state conditions with line current at ampacity (i.e. set $f_{ij}^{\text{loss}*} = R_{ij}(I^{\text{lim}})^2$, with R_{ij} the resistance per unit length [Ω/m].) Values T_{amb}^*, q_s^* describe representative ambient conditions, and may be obtained from forecasts, measurements or historical records. Thus, linearization of (25), together with forward Euler discretization, yields:

$$\Delta T_{ij}[k+1] = \tau_{ij} \Delta T_{ij}[k] + \rho_{ij} \Delta f_{ij}^{\text{loss}}[k] + \delta_{ij} \Delta d_{ij}[k], \qquad (26)$$

where

$$\tau_{ij} = 1 - \frac{T_s \bar{\gamma}_c}{mC_p}, \qquad \bar{\gamma}_c = \eta_c + 4\eta_r(T^{\text{lim}} + 273)^3, \quad (27)$$

and $\rho_{ij} = \frac{T_s}{mC_p}$ [°C-m/W]. The effects of exogenous inputs are captured by $\delta_{ij} = [\rho_{ij}\ \gamma_{ij}]$, where

$$\gamma_{ij} = \frac{T_s \bar{\gamma}_a}{mC_p}, \qquad \bar{\gamma}_a = \eta_c + 4\eta_r(T^*_{\text{amb}} + 273)^3, \qquad (28)$$

and $\Delta d_{ij} = \text{col}(\Delta q_{s,ij}, \Delta T_{\text{amb}})$. Note that $\Delta q_{s,ij}$ is a function of conductor diameter and solar input. Numerical stability requires that $\tau_{ij} \in (-1, 1)$, $\forall ij$, which implies the sampling time must satisfy $T_s < \min_{ij}\{2\frac{mC_{p,ij}}{\bar{\gamma}_{c,ij}}\}$. That is, the choice of controller sampling time T_s is determined based on the fastest linearized line-temperature time-constant.

Remark III.7. The MPC mitigation scheme seeks to drive line temperatures below limits (subject to the lossy DC model), but once below limits there is no incentive to lower temperatures further. That is, MPC should compute control actions that only take into account lines with $\Delta T_{ij} > 0$. Thus, a measure of temperature that aligns with such an objective is given by $\Delta \hat{T}_{ij} = \max\{0, \Delta T_{ij}\}$. This constraint can be relaxed to the linear formulation,

$$0 \le \Delta \hat{T}_{ij} \qquad (29a)$$
$$\Delta T_{ij} \le \Delta \hat{T}_{ij}. \qquad (29b)$$

Because the objective function penalizes $\Delta \hat{T}_{ij}$, this relaxation will always be tight.

To ensure correct temperature dynamics in (26), the convex relaxation of line losses given by (17) must be tight whenever a line's temperature rises above its limit (i.e. $\Delta T_{ij} > 0$). The following theorem establishes this crucial result.

Theorem III.8. (Temperature and Convex Relaxation.) Assume $g_{ij} > 0$ and losses in (22) are fixed to a predetermined value, according to (23), over the duration of the prediction horizon. If the temperature of line $(i, j) \in \mathcal{E}$ exceeds its limit at time $l + 1$, then the convex relaxation (17) is tight with respect to line (i, j) for all previous time-steps. That is, if $\exists l \in \mathcal{M}$ and $(i, j) \in \mathcal{E}$ such that $\Delta T_{ij}[l+1] > 0$, then adjacency conditions are satisfied for (17a) and $\theta^+_{ij}[\kappa]\,\theta^-_{ij}[\kappa] = 0$, $\forall \kappa \le l$. Hence the convex relaxation associated with line (i, j) is tight $\forall \kappa \le l$.

Proof. The full proof is given in Appendix B. To sketch the proof, let $\{\Delta T_{ij}[l]\}^M_{l=1}$ be an optimal MPC temperature trajectory for line (i, j) and assume $\exists l \in \mathcal{M}$ such that $\Delta T_{ij}[l + 1] > 0$ but the solution is *not* tight for some $\kappa \le l$. That is, losses are overestimated via the convex relaxation (i.e. $\theta^+_{ij}[\kappa]\,\theta^-_{ij}[\kappa] > 0$ and/or adjacency conditions are not satisfied in the PWL relaxation, see Fig. 3). Then a feasible solution can be derived which is identical to the optimal solution except that it enforces a tight formulation at time κ and reduces line losses accordingly, say from $f^{\text{loss}}_{ij,\text{relax}}[\kappa] > f^{\text{loss}}_{ij,\text{tight}}[\kappa]$. According to (26), decreased losses at time κ result in lower temperature at later times, which implies that the temperature overload at time $l + 1$ must be less under the tight feasible solution. Since the objective function penalizes $\Delta \hat{T}_{ij}[\kappa]$, the feasible

tight trajectory provides a lower cost solution than the relaxed optimal trajectory. This is a contradiction. Thus, if (i, j) has a temperature overload at time $l + 1$, the formulation is locally tight $\forall \kappa \le l$. $\qquad\square$

Remark III.9. (From DAE to ODE.) The DAE system presented in (2) cannot be expressed as an ordinary differential equation (ODE) system, because there is no bijective transformation between algebraic and dynamic states. This is because the convex relaxations employed in the MPC model beget multiple optimal algebraic solutions for lines that satisfy $\Delta T_{ij} \le 0$. Thus, the algebraic set of equations in (2c) has singular $\hat{F}$. Theorem III.8 yields conditions which ensure a locally unique solution for lines that exhibit temperature overloads, thus providing the basis for MPC to take meaningful action against such overloads.

E. MPC implementation

Given the complete controller model description, the state and input vectors can be collated:

$$x = \text{col}\{\Delta \hat{T}, E, f_G\} \qquad (30a)$$
$$u = \text{col}\{\Delta f_G, f^{\text{spill}}_{G_W}, f^{\text{red}}_D, f_{Qc}, f_{Qd}, \psi\} \qquad (30b)$$
$$z = \text{col}\{\theta, \theta^+, \theta^-, \theta^{PW}, f, f^{\text{loss}}, f_D, f_{G_W}, f_Q\}. \qquad (30c)$$

The objective of the MPC scheme is to determine the optimal control actions that alleviate temperature overloads $\Delta \hat{T}_{ij}$, while minimizing deviations from the economic set-points established by Level 1. Accordingly, the MPC objective function is composed of the terms:

$p_o(\Delta \hat{T}_{ij}[l|k])^2$ - line temperature overload

$p_g(f_{Gn}[l|k] - f^{\text{sp}}_{Gn,k+l})^2$ - generation output deviation

$p_r(\Delta f_{Gn}[l|k] - \Delta f^{\text{sp}}_{Gn,k+l})^2$ - generation ramping

$p_e(E_n[l|k] - E^{\text{sp}}_{n,k+l})^2$ - SOC deviation

$p_q(f_{Qd/c,n}[l|k] - f^{\text{sp}}_{Qd/c,n,k+l})^2$ - dis/charging deviation

$p_s(f^{\text{red}}_{Dn}[l|k])^2$ - demand response

$p_w(f^{\text{spill}}_{Gwn}[l|k])^2$ - wind spill

$p_p(\psi_{ij}[l|k] - \psi^{\text{sp}}_{ij,k+l})^2$ - PST reference deviation

where reference values, denoted $(\cdot)^{\text{sp}}$, refer to the economically optimal set-points computed in Level 1. Based on the MPC objectives and the state and input definitions in (30), the weighting matrices in (2a), (3) are given by:

$$Q = \text{diag}\left\{p_o I, \frac{p_e}{10M^2}I, \frac{p_g}{10M^2}I\right\} \succ 0 \qquad (31a)$$
$$S_M = \text{diag}\{p_o I, p_e I, p_g I\} \succ 0 \qquad (31b)$$
$$R = \text{diag}\{p_r I, p_w I, p_s I, p_q I, p_q I, p_p I\} \succ 0 \qquad (31c)$$

where I represents square identity matrices of appropriate dimensions, diag$\{\cdot\}$ is a block-diagonal matrix, and $\succ 0$ denotes positive-definiteness. Note that the terminal cost matrix S_M penalizes deviations from economical references for storage SOC and conventional generation states more severely than does the running-cost weighting matrix Q. This is because MPC does not care *how* these reference signals are tracked,

only that they are being considered by the end of the horizon. The objective function weighting factors must be tuned to achieve the desired MPC response.

To bring line temperatures at or below their limits by the end of the prediction horizon, a terminal constraint is employed:

$$\mathcal{T}_x = \left\{ x \,\Big|\, \Delta\hat{T}[M] = 0; E[M] \in [0, \overline{E}]; f_G[M] \in [\underline{f_G}, \overline{f_G}] \right\}. \tag{32}$$

Note that $\mathcal{T}_x$ is compact and contains the "origin", established by line temperature limits and Level 1 reference values. The remainder of the controller description (2) follows directly from the model details presented in Section III.

Remark III.10. (Stability and controllability.) Despite the controller consisting of a linear model together with terminal constraints and penalties, ensuring stability of the proposed hierarchical control scheme (Level 1 and Level 2) is not straightforward. Few systematic analysis methods are available for guaranteeing performance [30]. Furthermore, the DAE singularity discussed in Remark III.9 limits application of standard state-space results.

It is assumed that the controllable resources defined in (30b) exert a non-negligible influence on the power flowing through overloaded lines. That may not be the case if an overloaded line is remote from all the available resources. This controllability can be assessed by evaluating sensitivities, such as "generation shift factors" [18], for the lines in question.

F. Data management and communication

The MPC control scheme requires a model of the network, together with measurements of the conductor temperature of (potentially) overloaded lines, SOC of energy storage devices, output power from both conventional and renewable generation, power demand, and PST angles[2]. These data establish the initial point for the MPC prediction trajectory, and therefore must be updated every time MPC reinitializes, at the time-step T_s. These measurement requirements are consistent with existing energy management system (EMS) capabilities, with topology processing establishing the network model, and state-estimation providing generation and load information. Technology for measuring conductor temperature is available, though telemetry of such measurements is not currently common. It is argued in [12] and references therein, in the context of dynamic line rating, that gathering line temperatures is quite feasible. Also, a trivial modification to the MPC formulation would allow some lines to be subject to standard (hard) power flow limits, while modeling temperature dynamics for lines that were outfitted with temperature sensors. Participation of energy storage devices in electricity markets will likely require telemetry of their SOC. This is already the case in NYISO [31].

In addition to well defined initial conditions, MPC prediction also requires forecasts of demand, the power available from renewable generation sources, and the ambient weather conditions governing line temperatures. Generation and load forecasts are already available and used in EMS contingency

---

[2]More generally, the operating points of all FACTS devices would be required.

analysis. Short-term weather forecasts are also typically available. Given that the MPC prediction horizon will generally be on the order of 15-30 minutes, a persistence forecast (which assumes those external influences remain unchanged) will often be adequate.

MPC broadcasts control signals at an interval of T_s, which is much slower than other controls, such as AGC [32]. Thus the input/output communications and data management requirements of the MPC scheme are consistent with the capabilities of existing EMS installations.

G. Case study

Simulation of the MPC scheme is described in Part II [1]. That paper considers a case study that is based on the IEEE RTS-96 test system [33], augmented to include energy storage and wind generation.

IV. SUMMARY AND FUTURE WORK

A bilevel hierarchical control scheme is proposed for managing contingencies in electric power systems. The scheme balances economic and security objectives through the use of a higher-level optimal scheduling process and a lower-level model predictive control (MPC) strategy. The MPC design rejects disturbances (contingencies) while tracking the optimal set-points established by the higher level. Disturbance rejection exploits the thermal overload capability of transmission lines. This allows time for adjustments to be made to controllable resources that include generation levels, energy storage and demand response.

A convex relaxation is applied to the AC power flow to develop a piece-wise linear approximation for line losses. This formulation is proven to be sufficient to enable MPC to drive line temperatures below limits. As supported by the IEEE RTS-96 case study analyzed in Part II [1], the proposed MPC scheme can significantly improve system reliability and economic performance by leveraging the temporal nature of energy storage and conductor temperatures.

The DC power flow used in the MPC development does not consider voltage magnitudes (nor reactive power). There is value in being able to include voltage information in a linear/convex MPC scheme as that would facilitate a more integrated approach to protecting against voltage collapse. To accomplish this, convex relaxations and cutting plane methods will be explored [34].

V. ACKNOWLEDGEMENTS

APPENDIX A
SIMULTANEOUS CHARGING AND DISCHARGING

In order to compare simultaneous charge/discharge behavior with complementarity-based charging, define their respective actions by the superscripts $(.)^S$ and $(.)^C$. Then for a given optimal storage device action the following holds:

$$f_{Qc}^C[l] - f_{Qd}^C[l] =: f_Q^* := f_{Qc}^S[l] - f_{Qd}^S[l]. \tag{33}$$

Note that there exists only one unique complementarity-based control action (due to the condition $f_{Qc}^C[l]f_{Qd}^C[l] \equiv 0$). However, without complementarity (i.e. under the simultaneous charge/discharge formulation), multiple solutions may exist. One side-effect of allowing simultaneous charge/discharge events is identified by the following:

Theorem A.1. For a given optimal storage flow $f_Q^*[l]$, the simultaneous charge/discharge model (compared with the complementarity-based model) underestimates SOC (i.e. $\Delta E[l+1] := E^C[l+1] - E^S[l+1]$) by

$$\Delta E[l+1] = T_s \frac{1-\eta_c\eta_d}{\eta_d} \sum_{m=0}^{l} \min \left\{ f_{Qc}^S[m], f_{Qd}^S[m] \right\}. \quad (34)$$

Proof. The proof follows directly from considering the two cases: $f_{Qc}^C \equiv 0$ and $f_{Qd}^C \equiv 0$. □

From the theorem, it is straightforward to see that the simultaneous charge/discharge model exactly matches the complementarity-based model when one of the following holds:

- $\eta_c = \eta_d = 1$ (perfect efficiency)
- $\min\{f_{Qc}^S[l], f_{Qd}^S[l]\} = 0$ (complementarity is satisfied)
- $f_Q^*[l] = \overline{f_Q}$

where $\overline{f_Q} \equiv \overline{f_{Qc}} = \overline{f_{Qd}}$ has been assumed for presentation clarity. (Generalization to $\overline{f_{Qc}} \neq \overline{f_{Qd}}$ is straightforward.) The last condition stems from

$$\min\{f_{Qc}^S[l], f_{Qd}^S[l]\} \in \left[0, \overline{f_Q} - f_Q^*[l]\right]. \quad (35)$$

This means that the controller can (erroneously) employ simultaneous charge/discharge to achieve a lower-than-actual SOC, which could be advantageous to reduce the cost of SOC deviations from the Level 1 reference. Furthermore, the controller can utilize simultaneous charge/discharge to reduce line overloads by fictitiously "burning" excess power through energy storage inefficiencies ($\eta_c, \eta_d < 1$).

To reduce the effect and occurrence of simultaneous charge/discharge events, two steps have been implemented. Firstly, to reduce the worst-case behavior of the simultaneous charge/discharge formulation, the following constraint is utilized:

$$\frac{f_{Qc,n}[l|k]}{\overline{f_{Qc,n}}} + \frac{f_{Qd,n}[l|k]}{\overline{f_{Qd,n}}} \leq 1 \qquad \forall l, k, n, \quad (36)$$

where $\overline{f_{Qc,n}}$, $\overline{f_{Qd,n}}$ are the rate limits on charging and discharging, respectively.

Secondly, most devices at most time-steps will satisfy $f_{Qn}[l|k] \neq 0$. This knowledge can be used to enforce complementarity-like constraints, and limit occurrences of simultaneous charge/discharge events. When MPC first runs, the charge/discharge status of storage devices over the prediction horizon is most likely unknown. In order to initialize the status, simultaneous charging/discharging is permitted for that first prediction trajectory. When MPC next runs, at time k, the charge/discharge status of each storage device over the prediction horizon is determined from its status at the corresponding time-step in the previous prediction trajectory (i.e. $k-1$). It should be noted that the prediction horizon at

time-step $k-1$ only extends to $f_{Qn}[M-1|k-1]$, so no prior value is available for initializing the status of $f_{Qc,n}[M-1|k]$ and $f_{Qd,n}[M-1|k]$. Therefore, the Level 1 status at the corresponding time can be used to establish the charging state for all devices at this terminal time-step. Fig. 4 outlines the algorithm employed in MPC.

1: *Initialize:* set $\alpha_{tol} \geq 0$
2: **if** $k = 0$ **then**   ▷ MPC first run: allow simulcharge
3:     **for** $l = 0, 1, \ldots, M-1$ **do**
4:         $f_{Qc,n}[l|k], f_{Qd,n}[l|k]$ satisfy (36)
5:     **end for**
6: **else**
7:     **for** $l = 0, 1, \ldots, M-2$ **do**
8:         **if** $f_{Qn}[l+1|k-1] > \alpha_{tol}$ **then**
9:             $f_{Qd,n}[l|k] = 0, \ f_{Qc,n}[l|k] \in [0, \overline{f_{Qc,n}}]$
10:         **else if** $f_{Qn}[l+1|k-1] < -\alpha_{tol}$ **then**
11:             $f_{Qc,n}[l|k] = 0, \ f_{Qd,n}[l|k] \in [0, \overline{f_{Qd,n}}]$
12:         **else**   ▷ Possible transition: allow simulcharge
13:             $f_{Qc,n}[l|k], f_{Qd,n}[l|k]$ satisfy (36)
14:         **end if**
15:     **end for**   ▷ Terminal control
16:     set $f_{Qc,n}[M-1|k] = 0$ or $f_{Qd,n}[M-1|k] = 0$
            according to Level 1 status
17: **end if**

Fig. 4. Reducing the effect of simultaneous charge/discharge for Level 2 MPC at time-step k.

Remark A.2. This algorithm introduces a delay of one time-step in the transition of storage devices from charging to discharging, or vice-versa. To address this issue, computation of the MPC trajectory for time k can be repeated using the latest status information. At this re-run, storage devices with $f_{Qn}[l|k] \in [-\alpha_{tol}, \alpha_{tol}]$ are handled in accordance with line 13 in Fig. 4.

To summarize, constraint (36) limits the worst-case behavior of simultaneous charge/discharge, and the algorithm in Fig. 4 reduces the frequency of simultaneous charge/discharge events. Thus, these two steps make the model more representative of reality, but at a slightly increased computational cost.

APPENDIX B
PROOF OF THEOREM III.8

Proof. Let $l+1$ be the predicted time when line (i,j) exceeds its temperature limit. Pick an arbitrary $\kappa \leq l$. Since the MPC problem embodies a QP problem (with linear constraints), it satisfies the Linearity/Concave Constraint Qualification trivially and the Karush-Kuhn-Tucker (KKT) first-order conditions are therefore necessary conditions for (global) optimality [35]. The KKT conditions relating variables $\{\theta_{ij}^+[\kappa], \theta_{ij}^-[\kappa], \theta_{ij}^{\text{PW}}(s)[\kappa]\}$ for any $\kappa \leq l$ and $\Delta \hat{T}[l+1]$ give the following

$$\theta_{ij}^+[\kappa] : 0 = -\lambda_1 + \mu_1 - \mu_2 - \underline{\mu}_5 \tag{37}$$

$$\theta_{ij}^-[\kappa] : 0 = -\lambda_1 - \mu_1 + \mu_2 - \underline{\mu}_6 \tag{38}$$

$$\theta_{ij}^{\text{PW}}(s)[\kappa] : 0 = \lambda_1 + \overline{\mu}_3^s - \underline{\mu}_4^s + \alpha_{ij}(s)(\mu_7^l \varphi_{ij,l-\kappa} + \zeta_{ij,\kappa}) \tag{39}$$

$$\Delta\hat{T}_{ij}[l+1] : 0 = 2p_o \Delta\hat{T}_{ij}[l+1] - \mu_7^l - \underline{\mu}_8^l \tag{40}$$

where

- $\lambda_1 \in \mathbb{R}$ – multiplier related to constraint that couples absolute value and PWL variables in (17b);
- $\mu_1 \in \mathbb{R}^+$ – multiplier related to upper bound for $\hat{\theta}_{ij}$;
- $\mu_2 \in \mathbb{R}^+$ – multiplier related to lower bound for $\hat{\theta}_{ij}$;
- $\overline{\mu}_3^s \in \mathbb{R}^+$ – multiplier related to upper bound for $\theta_{ij}^{\text{PW}}(s)$;
- $\underline{\mu}_4^s \in \mathbb{R}^+$ – multiplier related to lower bound for $\theta_{ij}^{\text{PW}}(s)$;
- $\underline{\mu}_5 \in \mathbb{R}^+$ – multiplier related to lower bound for θ_{ij}^+;
- $\underline{\mu}_6 \in \mathbb{R}^+$ – multiplier related to lower bound for θ_{ij}^-;
- $\mu_7^l \in \mathbb{R}^+$ – multiplier related to the inequality obtained by substituting temperature dynamics (26) into (29b).
- $\underline{\mu}_8^l \in \mathbb{R}^+$ – multiplier related to $0 \le \Delta\hat{T}[l+1]$ in (29a).
- $\varphi_{ij,l-\kappa} \in \mathbb{R}^+$ – constant based on $\Delta T_{ij}[l+1]$-to-$f_{ij}^{\text{loss}}[\kappa]$ transition from (26).
- $\zeta_{ij,\kappa} \in \mathbb{R}^+$ – linear combination of multipliers based on $\Delta T_{ij}[m]$-to-$f_{ij}^{\text{loss}}[\kappa]$ transitions ($\kappa \le m \le M-1, m \ne l$).

Lemma B.1. KKT condition (40) implies that $\mu_7^l = \beta\Delta\hat{T}_{ij}[l+1] \ge 0$ for some $\beta > 0$.

Proof. Consider two cases:
1) $\Delta\hat{T}_{ij}[l+1] = 0$: Then, $0 = -\mu_7^l - \underline{\mu}_8^l \Rightarrow \mu_7^l = \underline{\mu}_8^l = 0$ since $\mu_7^l, \underline{\mu}_8^l \ge 0$.
2) $\Delta\hat{T}_{ij}[l+1] > 0$: Then, $\underline{\mu}_8^l = 0$ due to complementarity, so $\mu_7^l = 2p_o\Delta\hat{T}_{ij}[l+1] > 0$ as $p_o > 0$.

Thus, $\underline{\mu}_8^l \equiv 0$ and set $\beta = 2p_o > 0$. The proof is concluded. $\square$

From the KKT conditions associated with $\theta_{ij}^+, \theta_{ij}^-$, it is straightforward to show that,

$$2\lambda_1 = -\underline{\mu}_5 - \underline{\mu}_6 \le 0. \tag{41}$$

This relationship will be used in Lemma B.2 to establish tightness of the convex relaxation of the absolute value constraint (i.e. $\theta_{ij}^+\theta_{ij}^- = 0$).

Lemma B.2. If line $(i,j) \in \mathcal{E}$ is predicted to exceed its temperature limit, then the absolute value complementarity relaxation is tight for all previous time-steps. That is, if $l \in \{0, \ldots, M-1\}$ such that $\Delta\hat{T}_{ij}[l+1] > 0$ then $\theta_{ij}^+[\kappa]\,\theta_{ij}^-[\kappa] = 0, \ \forall\kappa \le l$.

Proof. Let $\Delta\hat{T}_{ij}[l+1] > 0$, choose arbitrary $\kappa \le l$, and consider the following two cases:
1) Suppose $\sum_{s=1}^S \theta_{ij}^{\text{PW}}(s)[\kappa] = 0$, then from (17b), $\theta_{ij}^+[\kappa] = \theta_{ij}^-[\kappa] = 0$ and $\theta_{ij}^+[\kappa]\,\theta_{ij}^-[\kappa] = 0$.
2) Suppose $\sum_{s=1}^S \theta_{ij}^{\text{PW}}(s)[\kappa] > 0$, then $\exists s \in \{1, \ldots, S\}$ such that $\theta_{ij}^{\text{PW}}(s)[\kappa] > 0$, so $\underline{\mu}_4^s = 0$. Using Lemma B.1 and (39), and re-arranging gives:

$$0 < \beta\Delta\hat{T}_{ij}[l+1]\varphi_{ij,l-\kappa} \le \frac{-\overline{\mu}_3^s}{\alpha_{ij}(s)} - \frac{\lambda_1}{\alpha_{ij}(s)}. \tag{42}$$

Since $\overline{\mu}_3^s \ge 0$ this implies $\lambda_1 < 0$. From (41), one or both of $\underline{\mu}_5, \underline{\mu}_6 > 0$, which implies that one or both of $\theta_{ij}^+[\kappa], \theta_{ij}^-[\kappa] = 0$, and hence $\theta_{ij}^+[\kappa]\,\theta_{ij}^-[\kappa] = 0$. Because $0 < \sum_{s=1}^S \theta_{ij}^{\text{PW}}(s)[\kappa] = \theta_{ij}^+[\kappa] + \theta_{ij}^-[\kappa]$, only one of $\theta_{ij}^+[\kappa]$ and $\theta_{ij}^-[\kappa]$ can be zero.

Since κ was arbitrary, it has been proven that for positive temperature overload at time $l+1$, the absolute value relaxation is locally tight for all $\kappa \le l$. $\square$

Next, the goal is to prove that adjacency conditions are upheld in the relaxed formulation for all time-steps $\kappa \le l$ if $\Delta T_{ij}[l+1] > 0$. Chose arbitrary κ. To improve readability of the following argument, the notation "$[\kappa]$" will be dropped, though all notation is with respect to time-step κ.

Suppose $\theta_{ij}^{\text{PW}}(s) > 0$ for some $s > 1$. Then KKT condition (39) has $\underline{\mu}_4^s = 0$ and $\overline{\mu}_3^s \ge 0$, and so:

$$\mu_7^l \varphi_{ij,l-\kappa} + \zeta_{ij,\kappa} \le -\frac{\lambda_1}{\alpha_{ij}(s)}. \tag{43}$$

In order to establish a contradiction, suppose $\theta_{ij}^{PW}(s-1) \in [0, \Delta\theta)$. If $\theta_{ij}^{PW}(s-1) = 0$, then $\overline{\mu}_3^{s-1} = 0$ and $\underline{\mu}_4^{s-1} \ge 0$, so (39) implies that,

$$\mu_7^l \varphi_{ij,l-\kappa} + \zeta_{ij,\kappa} \ge -\frac{\lambda_1}{\alpha_{ij}(s-1)} > -\frac{\lambda_1}{\alpha_{ij}(s)}, \tag{44}$$

where the last strict inequality derives from strict monotonicity of $\alpha_{ij}(s) > 0$ over s, and the guarantee that $\lambda_1 < 0$ from Lemma B.2. This contradicts with (43). The proof that $\theta_{ij}^{PW}(s-1) \notin (0, \Delta\theta)$ is similar. Hence, $\theta_{ij}^{PW}(s) > 0 \Rightarrow \theta_{ij}^{\text{PW}}(s-1) = \Delta\theta$. Since κ was arbitrary, adjacency conditions are upheld for all $\kappa \le l$. Thus, the convex relaxation is locally tight for all time-steps prior to a line's temperature exceeding its limit. $\square$

REFERENCES

[1] M. Almassalkhi and I. Hiskens, "Model-predictive cascade mitigation in electric power systems with storage and renewables part II: Case-study," *IEEE Transactions on Power Systems*, submitted, 2013.

[2] W. A. Wulf, "Great achievements and grand challenges," *National Academy of Engineering - The Bridge*, vol. 30, pp. 5–10, Oct 2000.

[3] "Grid 2030 - a national vision for electricity's second 100 years," tech. rep., Federal Energy Regulatory Commission, July 2003.

[4] "Final report on the August 14, 2003 blackout in the United States and Canada: Causes and recommendations," tech. rep., US-Canada Power System Outage Task Force, Apr 2004.

[5] D. Mayne, J. Rawlings, C. V. Rao, and P. O. M. Scokaert, "Constrained model predictive control: Stability and optimality," *Automatica*, vol. 36, no. 6, pp. 789–814, 2000.

[6] F. Borrelli, A. Bemporad, and M. Morari, *Predictive Control for linear and hybrid systems*. 2013.

[7] G. Goodwin, M. Seron, and J. De Doná, *Constrained Control and Estimation: An Optimisation Approach*. Communications and control engineering series, Springer Science & Business Media, 2005.

[8] M. Larsson, D. J. Hill, and G. Olsson, "Emergency voltage control using search and predictive control," *Electrical Power and Energy Systems*, vol. 24, pp. 121–130, Feb 2002.

[9] M. Zima, P. Korba, and G. Andersson, "Power systems voltage emergency control approach using trajectory sensitivities," *IEEE Conference on Control Applications*, pp. 189 – 194, 2003.

[10] I. A. Hiskens and B. Gong, "MPC-based load shedding for voltage stability enhancement," *IEEE Conference on Decision and Control*, Dec 2005.

[11] P. Hines and S. Talukdar, "Controlling cascading failures with cooperative autonomous agents," *International journal of critical infrastructures*, vol. 3, no. 1, pp. 192–220, 2007.

[12] H. Banakar, N. Alguacil, and F. D. Galiana, "Electrothermal coordination part I: Theory and implementation schemes," *IEEE Transactions on Power Systems*, vol. 20, pp. 798–805, May 2005.

[13] N. Alguacil, H. Banakar, and F. D. Galiana, "Electrothermal coordination part II: Case studies," *IEEE Transactions on Power Systems*, vol. 20, pp. 1738–1745, Nov 2005.

[14] B. Otomega, A. Marinakis, M. Glavic, and T. Van Cutsem, "Emergency alleviation of thermal overloads using model predictive control," *PowerTech*, pp. 201–206, Jun 2007.

[15] J. Carneiro and L. Ferrarini, "Preventing thermal overloads in transmission circuits via model predictive control," *IEEE Transactions on Control Systems Technology*, vol. 18, no. 6, pp. 1406 – 1412, 2010.

[16] M. Almassalkhi and I. A. Hiskens, "Cascade mitigation in energy hub networks," *IEEE Conference on Decision and Control*, Dec 2011.

[17] M. Almassalkhi and I. A. Hiskens, "Impact of energy storage on cascade mitigation in multi-energy systems," *IEEE PES General Meeting*, Jul 2012.

[18] A. Wood and B. Wollenberg, *Power Generation, Operation, and Control*. Wiley-Interscience, second ed., 1996.

[19] A. L. Motto, F. D. Galiana, A. J. Conejo, and J. M. Arroyo, "Network-constrained multiperiod auction for a pool-based electricity market," *IEEE Transactions on Power Systems*, vol. 17, pp. 646–653, Aug 2002.

[20] M. Almassalkhi and I. A. Hiskens, "Optimization framework for the analysis of large-scale networks of energy hubs," *Power Systems Computation Conference*, Aug 2011.

[21] T. Van Cutsem and C. Vournas, *Voltage Stability of Electric Power Systems*. International series in engineering and computer science, Springer, 2007.

[22] "Voltage stability assessment: concepts, practices and tools." IEEE Special Publication SP101PSS, August 2002.

[23] I. Šmon, G. Verbič, and F. Gubina, "Local voltage-stability index using Tellegen's theorem," *IEEE Transactions on Power Systems*, vol. 21, no. 3, pp. 1267–1275, 2006.

[24] A. Monticelli, *State Estimation in Electric Power Systems: A Generalized Approach*. Springer, 1999.

[25] R. Palma-Benhke, A. Philpott, A. Jofré, and M. Cortés-Carmona, "Modelling network constrained economic dispatch problems," *Optimization and Engineering*, pp. 1–14, Oct 2012.

[26] J. Lee, *A first course in combinatorial optimization*. Cambridge University Press, 2004.

[27] L. Bai, J. Mitchell, and J.-S. Pang, "On convex quadratic programs with linear complementarity constraints," *Computational Optimization and Applications*, vol. 54, pp. 517–554, 2013.

[28] B. Lesieutre, D. Molzahn, A. Borden, and C. L. Demarco, "Examining the limits of the application of semidefinite programming to power flow problems," *Allerton Conference*, pp. 1492–1499, Oct 2011.

[29] IEEE Standard 738, *IEEE Standard for Calculating the Current-Temperature of Bare Overhead Conductors*, 2007.

[30] R. Scattolini, "Architectures for distributed and hierarchical Model Predictive Control – A review," *Journal of Process Control*, vol. 19, pp. 723–731, 2009.

[31] D. Allen, C. Brown, J. Hickey, V. Le, and R. Safuto, "Energy storage in the New York electricity market," tech. rep., NYISO, Dec 2009.

[32] N. Jaleeli, L. VanSlyck, D. Ewart, L. Fink, and A. Hoffmann, "Understanding automatic generation control," *IEEE Transactions on Power Systems*, vol. 7, pp. 1106–1122, August 1992.

[33] C. Grigg, P. Wong, P. Albrecht, R. Allan, M. Bhavaraju, R. Billinton, Q. Chen, C. Fong, S. Haddad, S. Kuruganty, W. Li, R. Mukerji, D. Patton, N. Rau, D. Reppen, A. Schneider, M. Shahidehpour, and C. Singh, "The IEEE reliability test system," *IEEE Transactions on Power Systems*, vol. 14, no. 3, pp. 1010 – 1020, 1999.

[34] C. Coffrin and P. Van Hentenryck, "A linear programming approximation of AC power flows," *INFORMS Journal of Computing*. To appear.

[35] M. S. Bazaara, H. D. Sherali, and C. M. Shetty, *Nonlinear Programming*. Wiley-Interscience, third ed., 2006.
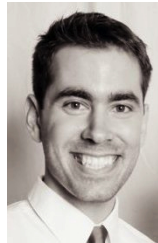
Mads R. Almassalkhi (S'06, M'13) received his B.S. degree in electrical engineering with a dual major in applied mathematics from the University of Cincinnati, Ohio, USA, in 2008, and an M.S. in electrical engineering: systems from the University of Michigan, Ann Arbor, USA, in 2010, where he obtained his Ph.D. degree from in 2013. His research interests include controls, optimization, power system analysis, and energy system modeling and he is a member of IEEE CSS and PES.

Ian A. Hiskens (F'06) received the B.Eng. degree in electrical engineering and the B.App.Sc. degree in mathematics from the Capricornia Institute of Advanced Education, Rockhampton, Australia, in 1980 and 1983 respectively, and the Ph.D. degree in electrical engineering from the University of Newcastle, Australia, in 1991.

He is the Vennema Professor of Engineering in the Department of Electrical Engineering and Computer Science, University of Michigan, Ann Arbor. He has held prior appointments in the Queensland electricity supply industry, and various universities in Australia and the United States. His research interests lie at the intersection of power system analysis and systems theory. His recent activity has focused largely on integration of renewable generation and controllable loads.

Dr. Hiskens is actively involved in various IEEE societies, and is VP-Finance of the IEEE Systems Council. He is a Fellow of the IEEE, a Fellow of Engineers Australia and a Chartered Professional Engineer in Australia.